

Corrosion Protection of Aluminum by Hydrophobization Using Nanoparticle Polymer Coatings Containing Plant Oil

Pieter Samyn*

University of Freiburg, Faculty of Environment and Natural Resources, Chair for Bio-based Materials Engineering, Werthmannstrasse 6, 79085 Freiburg, Germany

Um revestimento de polímero para proteção contra corrosão de superfícies de alumínio (AA 1050 A) foi avaliado, incluindo nanopartículas de maleimida-estireno sintetizadas em dispersão aquosa por imidização de poli(estireno-*co*-anidrido maleico) na presença de óleos vegetais (SMI/oil). Diferentes revestimentos de nanopartícula com gorduras mono e polinsaturadas foram avaliados através de espectroscopia Raman, medidas de ângulo de contato em água e microscopia de força atômica (AFM). Um tipo de nanopartículas com óleo de soja foi selecionado baseado na elevada reatividade do óleo e na formação de revestimento homogêneo com baixo teor de óleo livre, alto grau de imidização, alta hidrofobicidade e estabilidade a longo prazo. Após a otimização da composição do revestimento, as nanopartículas orgânicas foram misturadas com cera de carnaúba 20 wt.% e estireno/butadieno 50 wt.%, resultando em um ângulo de contato de 109°. As superfícies de alumínio foram pré-tratadas sob diferentes condições incluindo fosfatização ou condicionamento alcalino, e variação da velocidade de emersão. A melhor resistência à corrosão após teste do tipo *salt-spray* ocorre para amostras condicionadas por 10 s a 25 °C seguido de revestimento por imersão a 125 mm min⁻¹. A camada revestida resultante é relativamente fina, mas com boa resistência à corrosão em paralelo aos valores de ângulo de contato mais elevados e rugosidade da superfície um pouco mais elevada em relação aos revestimentos depositados a velocidades baixas.

A polymer coating for corrosion protection of aluminum surfaces (AA 1050A) was evaluated, including styrene maleimide nanoparticles synthesized in aqueous dispersion by imidization of poly(styrene-*co*-maleic anhydride) in presence of vegetable oils (SMI/oil). Different nanoparticle coatings with mono- and poly-unsaturated oils were evaluated through Raman spectroscopy, water contact angle measurements and atomic force microscopy (AFM). One type of nanoparticles with soy oil was selected based on the high oil reactivity and formation of homogeneous coating with low content of free oil, high degree of imidization, high hydrophobicity and long-term stability. After optimization of the coating composition, the organic nanoparticles were mixed with 20 wt.% carnauba wax and 50 wt.% styrene/butadiene, resulting in a contact angle of 109°. The aluminum surfaces were pre-treated under different conditions including phosphatization or alkaline etching, and dip-coating speed variation. The best corrosion resistance after salt-spray testing occurs for samples that were etched for 10 s at 25 °C, followed by dip-coating at 125 mm min⁻¹. The resulting coating layer is relatively thin, but with good corrosion resistance in parallel with the highest contact angle values and slightly higher average surface roughness than coatings deposited at low speeds.

Keywords: nanoparticles, polymer, oil, corrosion, hydrophobicity, aluminum

Introduction

The protection of solid surfaces that form a first interaction barrier with the environment, is a key issue for improving durability of materials in our daily life. The surface properties can be modified by various techniques and additives, but some of them are expensive,

contaminating or even toxic on long- or short-term. The development of sustainable and protective coatings should consider the replacement of contaminating and toxic moieties together with a reduction of solvents. Novel and sustainable methods providing corrosion resistance to metal surfaces may include renewables:¹ e.g., vegetable oils are abundantly available and can replace common chemical surface treatments for corrosion inhibition.² In parallel, aqueous-based protective coatings are preferred: recently,

*e-mail: pieter.samyn@fobawi.uni-freiburg.de

waterborne organic coatings were developed for protection of metallic substrates.^{3,4}

The application of nanotechnology offers new possibilities for the more rational use of raw materials and the development of more efficient and environmentally-friendly production methods. Especially, it provides tools to improve the functionalization and protection of surfaces: the nanoscale modification of surfaces allows for the precise localization of chemical moieties and incorporation of specific topographic features. As recently reviewed, nanoparticle additives enhance the corrosion resistance of zeolite, epoxy and antimicrobial coatings.⁵ Moreover, specific mesoporous nanoparticles were synthesized as nanocontainers including corrosion inhibitors that provide active corrosion protection through encapsulated agents,^{6,7} and self-healing effects.⁸

Inorganic nanoparticles deposited by sol-gel technology are most frequently used to form mechanically stable anti-corrosion coatings.⁹ As an advantage, coatings with inorganic nanoparticles can be sintered at low temperatures in presence of boron or sodium oxide, and were specifically developed for corrosion protection of magnesium alloys, forming a crack-free film with a thickness of several micrometers.¹⁰ As a disadvantage, nanoparticles have high tendency to agglomerate due to the high ratio of surface area to volume. Therefore, various stabilizers (surfactants, polymers, triblock polymers, proteins and carbohydrates) have been used for the synthesis of anti-corrosive Ag nanoparticles with various shapes and sizes.^{11,12} The corrosion resistance of hybrid composite coatings was improved in presence of nanoparticles such as, e.g., TiO₂,^{13,14} Cu₂O,¹⁵ ZnO,¹⁶ ZrO₂,¹⁷ Fe₃O₄,¹⁸ SiO₂,¹⁹ CeO₂,²⁰ and Au.²¹ Many of them have been applied as additives in waterborne acrylic or epoxy coatings.^{22,23} Also rare earth oxide nanoparticles improve the corrosion resistance of *in situ* phosphatized organic coatings.²⁴ Otherwise, inorganic nanoparticles such as SiO₂, Zn and Fe₂O₃ have been mixed with an epoxy coating,^{25,26} or TiO₂ nanoparticles were added to epoxy-polyaniline coatings,²⁷ to improve the microstructure of the coating matrix and thus enhance both the anti-corrosive performance and mechanical properties. Specific surface textures are often developed through the self-assembly of films with Au or Ag nanoparticles, which contribute to corrosion inhibition of copper surfaces.²⁸ In general, the formation of a protective barrier layer is an initial requirement for corrosion protection, as demonstrated for hybrid sol-gel coatings of SiO₂-methacrylate coatings doped with TiO₂-CeO₂ nanoparticles.²⁹

The corrosion resistance of Mg-based nanoparticles specifically depends on the atmosphere, as the formation of an amorphous carbon-doped surface in CH₄ atmosphere

provides best protection.³⁰ Therefore, it can be of interest to further explore the corrosion resistance of organic nanoparticle coatings in parallel with their low toxicity and delivery under aqueous condition. However, the application of organic nanoparticles for corrosion protection remains limited. In one example, urea-modified montmorillonite clay nanoparticles have been added as additives into an epoxy resin, resulting in better corrosion resistance within optimum percentage ranges.³¹ Otherwise, nanoclay dispersions,^{32,33,34} or polyaniline waterborne latex nanoparticles,^{35,36} have been used as pure additives or in combination with TiO₂ nanoparticles.³⁷ On the other hand, the organic nanoparticles should not deteriorate the mechanical surface properties (e.g., plasticization) and therefore, they should have high glass transition temperature.

A first requirement in the formation of surface layers for passive corrosion protection is the creation of a hydrophobic film, which might provide additional resistance in severe corrosive media due to reduced wetting and less direct contact with water and/or corrosive liquids. In one example, superhydrophobic aluminum surfaces were created by deposition of a chitosan layer and poly(octadecene-*alt*-maleic anhydride) on microroughened substrates.³⁸ In the present work, we explore alternative applications for organic nanoparticle coatings of imidized poly(styrene-*co*-maleic anhydride) that were previously used for the hydrophobic protection of paper surfaces.³⁹ As a main new application area, they can be applied as additives for corrosion protection of aluminum surfaces. Therefore, the coating should show good reactivity and adsorption to the metal substrate. First, an appropriate organic coating composition including nanoparticles with vegetable oils, latex binder and carnauba wax will be selected in order to maximize the hydrophobicity and stability. Also the pre-treatment for aluminum surfaces and coating deposition parameters will be further analyzed in order to provide optimum corrosion protection.

Materials

Coating composition

A poly(styrene-*co*-maleic anhydride) copolymer or SMA with 26 mol% maleic anhydride and molecular weight $M_w = 80.000 \text{ g mol}^{-1}$ was obtained from Polyscope (Geleen, The Netherlands). In addition, different refined vegetable oil types including soy oil (SoyO), high-oleic sunflower oil (SunfO), corn oil (CornO), castor oil (CastO), rapeseed oil (RapsO) and hydrogenated castor oil (HCastO) were used from Cargill Agricola S/A (Mairinque, Brazil). Ammonium hydroxide was obtained from Belgocare (Niel, Belgium) and used as a 25% aqueous solution (0.9 g mL⁻¹).

Organic nanoparticles with encapsulated vegetable oils were synthesized by Topchim N.V. along a previously published protocol,⁴⁰ where SMA was imidized into poly(styrene-*co*-maleimide) or SMI in presence of vegetable oil. In brief, the SMA was loaded in a laboratory-scale autoclave together with a selected type of vegetable oil, ammonium hydroxide and water. The weight ratio of oil to SMA was 1:1, while the ratio of ammonium hydroxide to maleic anhydride was 1:1. After 4 hours reaction time under continuously stirring at 160 °C and a maximum pressure of 6 bar, the reaction mixture was cooled to room temperature and evacuated from the autoclave reactor. As a result, SMI/oil nanoparticles were obtained in a homogeneous aqueous dispersion without any phase separation between the oil and organic phase. The SMI/oil nanoparticle dispersions have good stability with a zeta potential $\zeta = -40$ mV. Some technical characteristics of the SMI/oil nanoparticle dispersions are summarized in Table 1. The reported particle size measurements were obtained from dynamic light scattering (in dispersion). The solid content (S.C.) was experimentally determined after infrared drying of the dispersions and equals 50 wt.%, which is in good agreement with the theoretical calculations based on the reactor loadings.

The final polymer coating for corrosion protection consists of a selected SMI/oil nanoparticle type, mixed with carnauba wax (Carbonos do Brazil Ltda, Brazil) and styrene butadiene (SB) latex (DIC, Germany). The SB latex is delivered as a water-based emulsion of styrene-butadiene copolymer particles (200-250 nm) with 60 wt.% styrene monomer and 40 wt.% butadiene monomer. After a systematic variation in contents, the optimum amounts of wax (20 wt.%) and latex (50 wt.%) were selected in this study according to the required hydrophobicity and coating homogeneity.

Aluminum substrates and coating conditions

Aluminum alloy sheet surfaces (AA 1050A) were used, with a composition of Fe (0.185 wt.%), Si (0.109 wt.%)

and Al (balance). The substrates were ultrasonically cleaned in acetone and methanol, followed by drying in warm air, before being pre-treated along different methods as summarized in Figure S1. The surfaces were prepared by three methods, including (i) only degreasing, (ii) alkaline etching in 1M NaOH with variable bath temperatures of 25 to 60 °C, and etching times 2 to 120 s, or (iii) zinc phosphatization in a solution (pH = 3) of 85% H₃PO₄ (20 mL) + ZnO (7g) + NaF (0.8 g) at 25 °C during 3 minutes. From the variable surface preparations, optimum pre-treatment conditions were determined as discussed in relation with the test results.

The polymer coatings were applied by dip-coating in an aqueous dispersion of pure SMI/oil nanoparticles (determination of intrinsic hydrophobicity of the hybrid nanoparticle coatings) or in a dispersion of SMI/oil nanoparticles, carnauba wax, and SB latex. The coatings were applied by dipping the aluminum samples in a vial containing the coating dispersion and by withdrawing the samples at two constant velocities of 25 mm min⁻¹ or 125 mm min⁻¹. Before any further characterization, the coatings were dried for one day under room conditions (23 °C, 60% RH).

Experimental Methods and Characterization

The dispersions of SMI/oil nanoparticles and their coating after drying on the aluminum surface were chemically characterized by FT-Raman spectroscopy (Spectrum GX, Perkin Elmer). The Raman spectra of the dispersions or surfaces were collected as an average from 64 scans at a resolution of 4 cm⁻¹ between 4000 and 100 cm⁻¹ wavenumbers, using a Nd:YAG laser (1064 nm) with 500 mW power. The surfaces were further evaluated by either secondary scanning electron microscopy (Philips FEI XL30 SEM instrument) or optical microscopy (Olympus BX 51). The topography of nanoparticle coatings was further studied by tapping-mode atomic force microscopy (AFM), using PicoScan 2500 PicoSPM II Controller (PicoPlus, Molecular Imaging), using a silicon probe with

Table 1. Characteristics of aqueous nanoparticle dispersions including different types of vegetable oils (SMI/oil)

Oil Type	Name dispersion	pH	S.C. / %	Viscosity / cp	z-Average particle size, diameter / nm	Particle size (polydispersity)
Soy oil	SMI/SoyO	5.48	49.8	146	149	0.163
Sunflower oil	SMI/SunfO	5.38	48.8	134	143	0.176
Corn oil	SMI/CornO	5.44	49.9	102	143	0.161
Castor oil	SMI/CastO	5.72	49.9	230	148	0.137
Rapeseed oil	SMI/RapsO	5.43	49.5	91	156	0.137
Hydrogenated oil	SMI/HCastO	5.54	49.4	116	132	0.152

$k = 40 \text{ N m}^{-1}$ and 300 kHz resonant frequency. The average surface roughness (R_a) was determined from a 2D profile selected on a $2 \times 2 \mu\text{m}^2$ scan area (WSxM 5.0 Software).

The contact angles of D.I. water droplets were measured on a Digidrop equipment (GBX, France). The static contact angles were determined by placing a droplet with constant volume of $6 \mu\text{L}$ on the surface over a time of 60 seconds, and contact angle values were averaged from 10 measurements on different locations (where possible). In general, contact angles remained stable over time and contact angle readings were made immediately after deposition of the droplet. The dynamic contact angles were measured by modifying the droplet volume between 0 to $6 \mu\text{L}$ in contact with the surface, either increasing the volume (advancing contact angle θ_a) or reducing the volume (receding contact angle θ_r). This method is used for determining contact angles on nanostructured surfaces, because it is more sensitive to the local roughness and composition of the sample.

The corrosion resistance was evaluated with a salt spraying test on coated and X-shape scratched aluminum samples, according to the standard ASTM B117 (pressure 0.8 bar, temperature $35 \text{ }^\circ\text{C}$, 49% relative humidity). The positioning of the samples in testing chamber is illustrated in Figure S2. However, the testing standard does not provide specific information on the applied testing time or on the appearance of corrosion products under the form of salts. As the various coatings have different behaviour in the salt spray test, the final test duration was different from one to another type of coating depending on its corrosion resistance. The appearance of corrosion products was visually evaluated after exposure times of 120, 240, 360, and 480 hours.

The coating thickness was measured with a microprocessor coating thickness gauge, using a Minitest 2000 (Elektro-Physik, Köln, Germany). With this apparatus, the non-destructive thickness measurement of insulating coatings on non-ferrous materials is based on the eddy current principle (N-probes). The sample thickness was measured before and after the corrosion process in ten points, five on the front side (i.e., up side of the samples in Figure S2) and five on the back side (i.e., down side of the samples in Figure S2). The morphology of the coating cross-sections was also visually evaluated by secondary electron microscopy (SEM).

Results and Discussion

Chemical characterization of coating substances

First, the chemical compositions of the different SMI/oil nanoparticle dispersions (in water) and coatings (after

drying) were evaluated by Raman spectroscopy, in order to confirm the chemical interaction between the oil and the organic coating components together with the chemical quality of the nanoparticle coatings. After deposition of the coatings by dip-coating at low speeds (25 mm min^{-1}) and high speeds (125 mm min^{-1}), the aluminum substrates were homogeneously covered. Therefore, the viscosity (see Table 1) of the nanoparticle dispersions was assumed to be compatible with the dip-coating conditions.

A detail of the Raman spectra for the original coating dispersions and dried coatings is shown in Figure 1, with an indication of the characteristic absorption bands for imide and styrene. After the imidization reaction, the maleic anhydride bands ($\text{C}=\text{O}$, 1860 cm^{-1}) disappeared in favour of the appearance of an imide I band ($\text{C}=\text{O}$, 1765 cm^{-1}). The chemical reaction of SMA in presence of ammonium hydroxide involves the ammonolysis (ring-opening) of the maleic anhydride moieties at low temperatures (90 to $120 \text{ }^\circ\text{C}$), followed by the formation of imide moieties by a ring-closing reaction of the ammonolyzed maleic anhydride. The imide starts to develop during chemical reaction at temperatures above $120 \text{ }^\circ\text{C}$ under aqueous conditions (Figure 1a) and further develops during drying (Figure 1b). In parallel, the styrene moieties (1602 cm^{-1}) remain relatively inert after synthesis, and related absorption bands were used for normalization of the spectra. The presence and reactivity of oil ($\text{C}=\text{O}$, 1750 cm^{-1} ; $\text{C}=\text{C}$, 1666 cm^{-1}) can be estimated from the variation in the band intensities related to the unsaturated double bonds, as these sites can be considered as reactive sites. The interaction between the oil and the organic phase after imidization, takes place in between the ammonolyzed maleic anhydride parts and the reactive double bonds of the fatty acids in the oil. The spectra after drying (Figure 1b) illustrate that the interactions between the oil and the imidized maleic anhydride further intensify due to the relative decrease in $\text{C}=\text{C}$ band intensities (1666 cm^{-1}). However, the exact iodine-values of the oils after chemical reaction are difficult to estimate due to an overlap with the imide-related absorption bands. A qualitative interpretation indicates an increase in iodine-value for oils as follows: SunfO, CastO, SoyO, CornO, RapsO, showing that SoyO (poly-unsaturated) is somewhat more reactive at the $\text{C}=\text{C}$ bonds, while CornO and RapsO (mono-unsaturated) are somewhat less reactive.

The degree of imidization for SMI/oil nanoparticles can be quantitatively calculated from the Raman band at 1765 cm^{-1} , relatively to the imidization of a completely imidized SMI sample that was obtained by thermal curing for 6 hours at $250 \text{ }^\circ\text{C}$. The maximum degree of imidization for a completely imidized SMI sample (26 mol% maleic

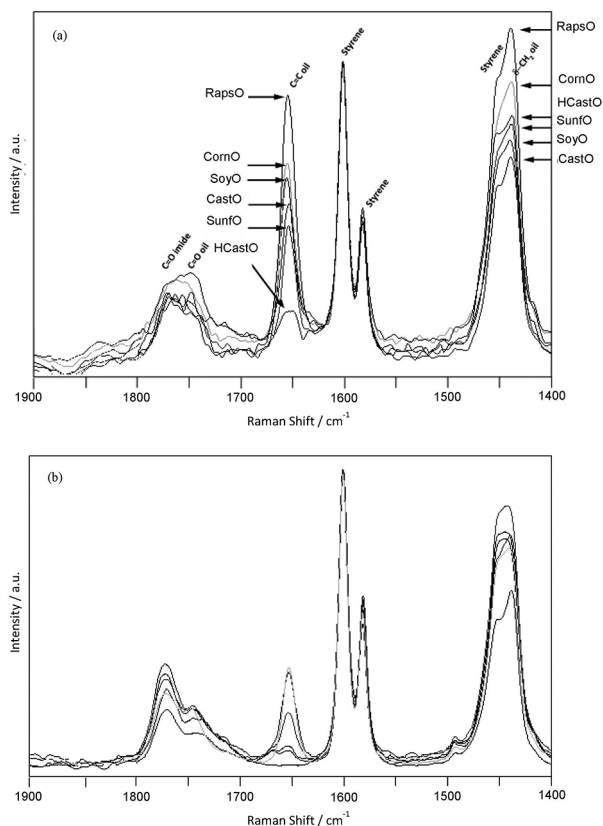


Figure 1. Chemical characterization of the nanoparticle coating substances by means of Raman spectroscopy. (a) SMI/oil nanoparticles in dispersion, (b) SMI/oil nanoparticles after coating and drying on aluminum.

anhydride, no oil) is 35% and is used as a reference value. The results for imidization of SMI/oil in aqueous dispersion and after drying as a coating on aluminum substrates, together with amounts of chemically reacted (and free) oil, are summarized in Table 2. All calculations were based on an average value for three spectra at independent places on the surface, with an overall standard deviation of $\pm 0.3\%$ on the imide content. After ageing of the coated samples for three months under environmental conditions (23 °C, 60% RH), a relatively similar degree of imidization was calculated (almost within the experimental error) and

confirms the good chemical stability of the coatings over time. Indeed, the imidized coatings do not further imidize as the temperature under environmental conditions is not high enough. Moreover, the high reactivity of SoyO as poly-unsaturated oil results in a low content of free oil, while the lower reactivity of mono-unsaturated or saturated oils results in higher free oil contents.

Hydrophobicity of nano-pigmented coating compositions

The hydrophobicity of SMI/oil nanoparticle coatings on aluminum substrates was evaluated in order to select an appropriate nanoparticle composition. Therefore, the aluminum substrates were prepared by alkaline pre-treatment (25 °C, 10 s) - details follow in next section - and SMI/oil nanoparticle coatings were deposited by dip-coating at 125 mm min⁻¹ from the aqueous nanoparticle dispersions. The static contact angle (θ_{stat}) and dynamic contact angles (advancing θ_a , receding θ_r) with water on coated aluminum were measured immediately after deposition and after three months ageing of the coated samples under room conditions (23 °C, 60% relative humidity), with results given in Table 3. All nanoparticle coatings have a higher contact angle than uncoated samples. Depending on the type of oil, there is a significant improvement in hydrophobicity with highest contact angles for saturated oil (HCastO). However, the latter is likely explained by the high amount of free oil for SMI/HCastO (see Table 2). Otherwise, the SMI/oil nanoparticle coatings with poly-unsaturated oil (e.g., SMI/SoyO) have very small amounts of free oil and also present relatively high contact angles with good stability in hydrophobic properties as a function of the time. For all coatings, there is a slight increase in the water contact angles after ageing with improved hydrophobicity.

The dynamic advancing contact angles are slightly lower than the static contact angle measurements, for all SMI/oil nanoparticle coatings immediately after coating and after ageing. The standard deviation on the advancing

Table 2. Degree of imidization for SMI/oil nanoparticles in aqueous dispersion and after drying as a coating on alkaline-etched aluminum surfaces (25 °C, 10 s)

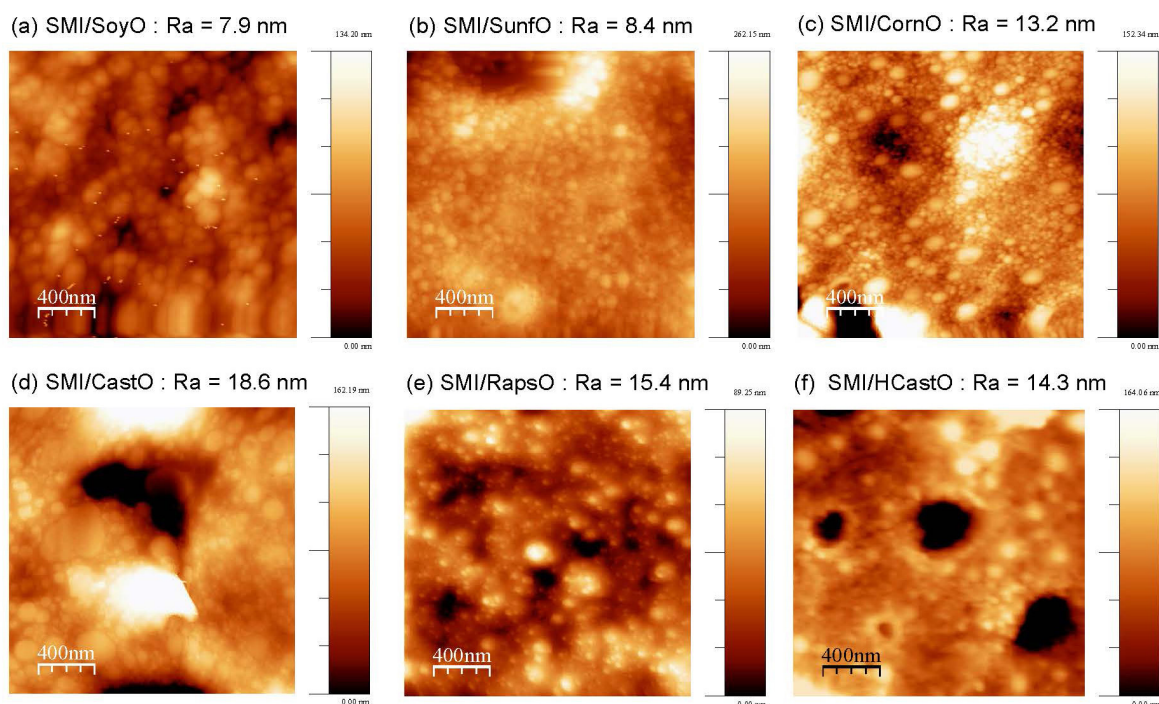
	In dispersion		Aluminum coating		
	Reacted oil content / %	Free oil content / %	Imide content / %	Imide content after coating / %	Imide content after ageing / %
SMI/SoyO	96	4	20.0	25.3	24.9
SMI/CornO	95	5	18.1	23.2	22.6
SMI/RapsO	85	15	16.3	20.3	20.2
SMI/SunfO	78	22	15.3	19.3	20.1
SMI/CastO	76	24	14.4	19.5	19.4
SMI/HCastO	68	32	17.2	24.1	23.8

Table 3. Water contact angles ($^{\circ}$) on alkaline-etched aluminum surfaces (25°C , 10 s) with different SMI/oil nanoparticle coatings, immediately after coating and after three months ageing

	Immediately after coating			After ageing		
	θ_{stat}	θ_a	θ_r	θ_{stat}	θ_a	θ_r
Uncoated	69 ± 0.8	64	40	69 ± 1.0	64	40
SMI/SoyO	88 ± 0.6	83	20	90 ± 0.8	84	40
SMI/SunfO	85 ± 0.5	82	15	89 ± 0.5	84	30
SMI/CornO	89 ± 0.7	85	20	91 ± 0.6	86	38
SMI/CastO	80 ± 1.1	72	30	82 ± 1.1	73	32
SMI/RapsO	92 ± 1.7	88	15	92 ± 1.5	84	25
SMI/HCastO	109 ± 1.2	106	34	108 ± 1.1	107	40

contact angles was larger compared to the static contact angles, and about $\pm 2^{\circ}$ for all measurements. In order to explain the differences between static and dynamic contact angles, the surface morphologies have to be taken into account. The values for advancing contact angles strongly depend on the surface roughness, as described in the Wenzel model for the apparent contact angles as a function of surface roughness. In general, the contribution of a higher surface roughness on hydrophobic surfaces augments the hydrophobicity, while a higher surface roughness on hydrophilic surfaces improves the surface hydrophilicity, relatively to a smooth surface. The present observation of slightly lower advancing contact angles relatively to the static contact angles indicates that there is

a slight contribution of the coating roughness decreasing the value for advancing contact angles on rough surfaces. The roughness of coated aluminum substrates is determined from AFM scans ($2 \times 2 \mu\text{m}^2$) for the different SMI/oil nanoparticle coatings (Figure 2). The values for the average surface roughness R_a of the coatings were determined from a 2D profile of the AFM scans, without performing any flattening procedure. Based on five measurements *per* surface scan, the standard deviation of average surface roughness was $\pm 0.5 \text{ nm}$. As a reference, the roughness for uncoated aluminum samples (alkaline etching) was $R_a = 4.2 \text{ nm}$. The roughness for coated samples ranges from $R_a = 7.9 \text{ nm}$ to $R_a = 18.6 \text{ nm}$: it is highest for SMI/CornO coatings and lowest for SMI/SoyO coatings. However,

**Figure 2.** Surface morphology of SMI/oil nanoparticle coatings on alkaline-etched aluminum surfaces (25°C , 10s) and values for average surface roughness R_a , including (a) SMI/SoyO, (b) SMI/SunfO, (c) SMI/CornO, (d) SMI/CastO, (e) SMI/RapsO, (f) SMI/HCastO.

the coatings of SMI/CornO, SMI/CastO, SMI/RapsO and SMI/HCastO have defects in their structure in the form of large holes, which likely develop due to local dewetting effects over the aluminum surface. The latter defects explain the higher roughness values. On the other hand, the coatings of SMI/SoyO and SMI/SunfO are more homogeneous, which is reflected in a low Ra-value.

Based on the evaluation of different SMI/oil nanoparticle dispersions and coating properties in Tables 2 and 3, we selected SMI/SoyO as a most appropriate composition with highest degree of imidization, resulting in relatively high contact angles and good stability over time. This is also supported by the high reactivity of SoyO and low free oil content, as illustrated in the Raman spectra. Moreover, a smooth surface coverage without local dewetting of the aqueous and oil phase was observed for SMI/SoyO. The latter is important to ensure the long-term stability and resistance of the coating.

In next steps, the selected SMI/SoyO nanoparticles were used as additives in a polymer coating. The composition of a polymer coating for corrosion protection of aluminum substrates should include a binder and additives in order to form a fully “closed” coating structure. Therefore, different amounts of SB latex and carnauba wax were added into the coating composition. After mixing the coating components, the homogeneous aqueous dispersion was suitable to be applied as a coating for all of the compositions. For the same pre-treatment conditions of the aluminum substrates as before (alkaline, 25 °C, 10 s) and dip-coating at 125 mm min⁻¹, the hydrophobicity of coatings with variable amounts of SMI/SoyO nanoparticles, SB latex and carnauba wax was evaluated. An overview of static water contact angle measurements (immediately after coating and after ageing) for different coating compositions is presented in Table S1. From these results, the hydrophobicity of the coating decreases after addition of SB latex, while it increases after adding carnauba wax. Due to the intrinsic drying effects of nanoparticle coatings as studied before,³⁹ the coating compositions with more than 50 wt.% SMI/SoyO nanoparticles provide inhomogeneous cracks. These cracks are due to the relatively high glass transition temperature T_g of the SMI/SoyO nanoparticles ($T_g = 165$ °C), preventing the diffusion of the particles into a homogeneous layer.⁴¹ On the other hand, the addition of SB latex provides a more homogeneous coating by filling the inter-particle space while it provides a smoother surface. The addition of carnauba wax as a hydrophobic agent is very efficient in further increasing the hydrophobicity of the coating. Based on this experimental data, an optimum coating composition was selected with 30 wt.% SMI/SoyO nanoparticles, 50 wt.% SB-latex and 20 wt.% carnauba

wax. Moreover, the water contact angles have good stability over time, indicating that there is no migration of nanoparticles. The coatings with higher amounts of carnauba wax have significantly lower contact angles after ageing, likely due to migration of the wax. The coatings with pure SB-latex or carnauba wax have lower contact angles than the composite coatings, confirming that the addition of SMI/SoyO nanoparticles clearly stimulates the hydrophobic effect.

The surface morphology of a polymer coating including SMI/SoyO nanoparticles, carnauba-wax and SB-latex on an aluminum substrate (alkaline etching at 25 °C, 10 s, deposition at 125 mm min⁻¹) is shown in Figure 3. The optical microscopy confirms that the substrate is homogeneously coated and a fully closed protective film is formed. The AFM scans ($2 \times 2 \mu\text{m}^2$) further confirm the presence of nanoparticles with elementary diameters of about 100 nm, and a good distribution of the nanoparticles within the coating. The phase contrast image provides important information on differences between the places where nanoparticles are located (high phase contrast response) and the locations in between (low phase contrast response) that are filled with binder and wax, forming a continuous coating.

The surface profile shows a nanometer range height variation on the surface that might promote the hydrophobic properties of the polymer coating. The average surface

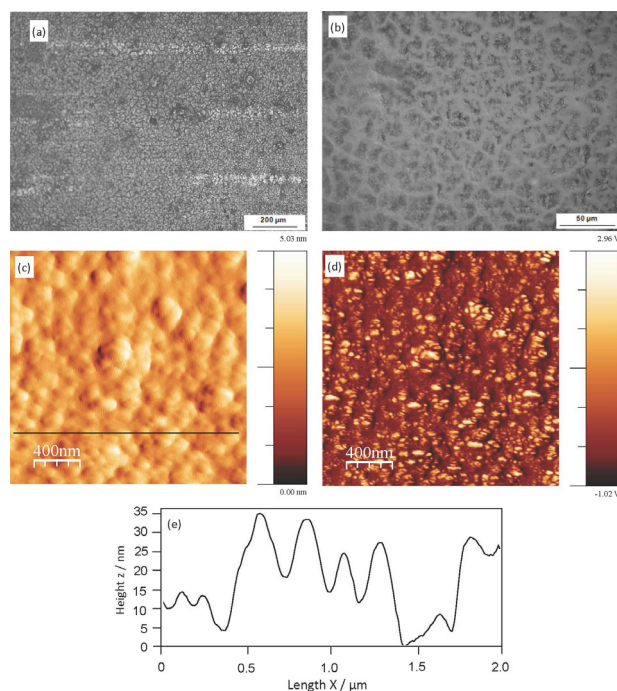


Figure 3. Surface morphology of a polymer coating including 30 wt.% SMI/SoyO nanoparticles, 50 wt.% SB-latex and 20 wt.% carnauba wax on aluminum substrates, (a, b) optical microscopy, (c) AFM height image, (d) AFM phase contrast image, (e) AFM profile along the profile line indicated in (c).

roughness of the polymer coating is $R_a = 6.8 \text{ nm}$: the homogenizing effect of the latex and carnauba wax results in a lower average surface roughness compared with the SMI/SoyO nanoparticle coating (Figure 2a).

Influences of aluminum substrate preparation

It is known that the surface pre-treatment of aluminum substrates has an important effect on the corrosion resistance of coated aluminum samples.⁴² In order to optimize the final corrosion performance, different pre-treatment conditions for the aluminum samples were evaluated. The aluminum substrates were first degreased, as this step finally provides a more homogeneous polymer coating than when the surfaces were not degreased. In general, the rolling process introduces scratches, kinks and foldings on the material surface, resulting in a deformed layer at the surface of about $1 \mu\text{m}$. Moreover, the top surface of rolled aluminum has different electrochemical reactivity than the bulk material. The top layer generally contains aluminum oxides and hydroxides and has more inclusions and cracks. Therefore, the substrates were etched under alkaline conditions in a solution of $\text{NaOH } 1 \text{ mol L}^{-1}$ for removal of the reactive top layer. All samples were prepared by gently stirring during the etching in order to get a more uniform surface.

The surfaces of pre-treated aluminum substrates under different alkaline etching conditions are analyzed by backscattered SEM images, as shown in Figure 4. The surfaces contain plate-shaped intermetallic compounds (Al_3Fe) with sizes of 0.2 to $7 \mu\text{m}$ and aspect ratio of 1 to 6 . Depending on the etching times ($2, 5, 10, 20, 30, 60, 120, 240$ seconds) and temperatures ($25, 40, 60 \text{ }^\circ\text{C}$), the amount of intermetallic particles adhering to the surface varies, with a minimum number of particles after 10 seconds. It was observed that the number of intermetallic deposits on the surface is higher after short etching times (5 seconds) and after longer etching times (30 seconds to 2 minutes). The latter phenomenon can be explained by preferential etching around the intermetallic inclusions and deposition on the aluminum surface if the sample remains too long immersed in the solution, as also observed in other studies.⁴³ The applied etching temperature does not significantly affect the final surface morphology. In conclusion, the best pre-treatment resulted to be alkaline etching during 10 seconds at room temperature ($25 \text{ }^\circ\text{C}$), rather than zinc phosphatization treatments.

Influences of coating conditions

The polymer coatings were deposited on pre-treated aluminum surfaces by dip-coating into the coating

dispersion. A survey study indicated that the dipping time had no significant effect, and only the influences of different controlled withdrawal speeds were further considered. After multiple essays, two speeds were selected: one slow (25 mm min^{-1}) and one five times faster (125 mm min^{-1}). The deposited coatings were dried during one day under room conditions ($23 \text{ }^\circ\text{C}$, $60\% \text{ RH}$).

A cross-section of the coated aluminum substrates under optimized conditions is shown in Figure 5. The cross sections of polymer coatings applied on aluminum substrates with different pre-treatments and under different dip-coating conditions are further detailed in Figure 6.

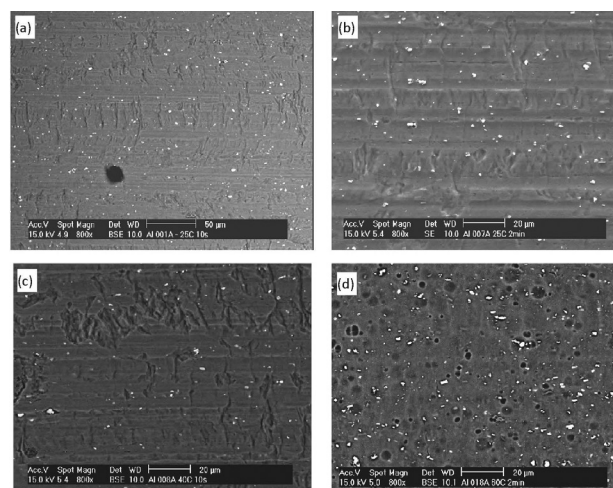


Figure 4. Surface morphology of aluminum substrates after alkaline etching under different conditions, including (a) 10 s, $25 \text{ }^\circ\text{C}$, (b) 120 s, $25 \text{ }^\circ\text{C}$, (c) 10 s, $40 \text{ }^\circ\text{C}$, (d) 120 s, $60 \text{ }^\circ\text{C}$.

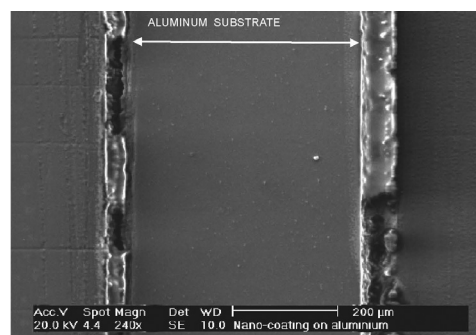


Figure 5. Cross-section of a coated aluminum substrate (AA 1050A), with optimized homogeneous coating morphology, deposited after etching substrates at $25 \text{ }^\circ\text{C}$ for 10 s, with dip-coating speed of 125 mm min^{-1} .

The automated measurements of coating thickness (Minitest 2000) are given in Table 4. The average surface roughness values R_a were determined from AFM scans ($2 \times 2 \mu\text{m}^2$), as illustrated before in Figure 3. By comparing qualitative SEM images and quantitative microprocessor data, there is a relatively good correspondence between measured thicknesses. However, the coating thickness measured by SEM seems to be slightly thicker and more

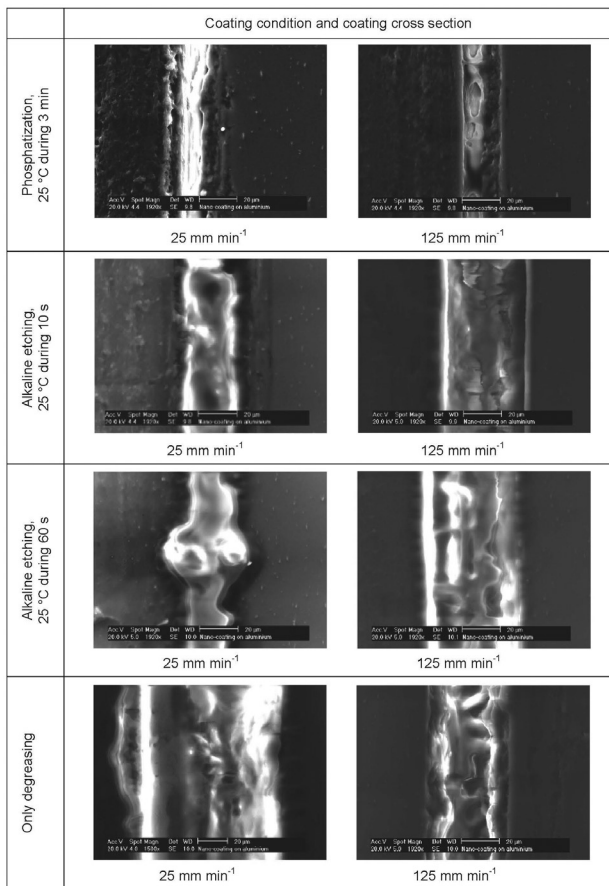


Figure 6. Cross sections of polymer coatings on aluminum substrates deposited after different pre-treatments with dip-coating speeds of 25 mm min⁻¹ and 125 mm min⁻¹.

influenced by local defects and scattering effects. Therefore, the thickness obtained by the microprocessor measurements was more reliable. The polymer coatings on phosphatized aluminum substrates are inhomogeneous under all conditions and not further detailed. For both phosphatized and alkaline surface pre-treatments, the polymer coatings deposited at 25 mm min⁻¹ are thicker than those deposited at 125 mm min⁻¹. For degreased samples, this trend is reversed

and can be attributed to inefficient removal of remaining contaminants during degreasing (see later, contact angle measurements), which cause dewetting of the coating over the aluminum surface when deposited at low speeds. After optimization of the dip-coating process in combination with alkaline pre-treatment (25 °C, 10 s), the coatings were ideally deposited with a speed of 125 mm min⁻¹, resulting in good homogeneity with average thickness of 6.5 μm and minimum standard deviation.

The static and dynamic water contact angles on pre-treated and coated aluminum substrates are evaluated in Table 5. The original aluminum surface is expected to be hydrophilic due to the high surface energy of metallic surfaces. The static contact angle of 69° for degreased aluminum substrates is relatively high, likely due to contamination effects from different hydrocarbons, which are present in normal air and will easily interact with metallic/oxidic surfaces based on their high surface energy. The contamination happens in relatively short periods also after an adequate degreasing pretreatment. After phosphatization and/or alkaline etching, the aluminum surfaces become more hydrophilic as a proof for the more efficient removal of surface contaminants. Then, the water drops easily spread over the aluminum surface and dynamic measurements are obviously meaningless (Table 5, ND = not determined). This means that the pre-treated aluminum surfaces after phosphatization or alkaline etching provide good wettability for coating with an aqueous polymer dispersion.

After deposition of the polymer coating and drying for 1 day under room conditions (25 °C, 60% relative humidity), the coated aluminum surfaces are hydrophobic. The samples that were pre-treated by etching at 25 °C during 10 seconds and coated at 25 or 125 mm min⁻¹ have highest hydrophobicity with contact angles of 103 to 109°: the high contact angle (109°) for the coating deposited at 125 mm min⁻¹ corresponds to a slightly higher roughness

Table 4. Polymer coating thickness and standard deviation averaged over six measuring points on aluminum samples with different coating conditions and pre-treatments (microprocessor measurements). Average surface roughness Ra on polymer coatings determined from AFM scans (2 × 2 μm²)

Aluminum pre-treatment	Coating condition	Mean coating thickness / μm	Standard deviation for coating thickness / μm	Average surface roughness Ra / nm
Phosphatization, 25 °C during 3 min	25 mm min ⁻¹	8.2	2.6	14.1
Phosphatization, 25 °C during 3 min	125 mm min ⁻¹	4.1	1.6	17.2
Alkaline etching, 25 °C during 10 s	25 mm min ⁻¹	8.0	3.2	4.3
Alkaline etching, 25 °C during 10 s	125 mm min ⁻¹	6.5	1.2	6.8
Alkaline etching, 25 °C during 60 s	25 mm min ⁻¹	10.2	3.2	9.4
Alkaline etching, 25 °C during 60 s	125 mm min ⁻¹	6.6	2.0	10.6
Only degreasing	25 mm min ⁻¹	17.0	6.4	18.9
Only degreasing	125 mm min ⁻¹	25.4	4.5	20.3

Table 5. Static and dynamic water contact angles ($^{\circ}$) on pre-treated aluminum substrates before and after coating with a polymer coating (SMI/SoyO + carnauba wax + SB latex)

Aluminum pre-treatment	Coating condition	Contact angles on pre-treated aluminum			Contact angles on coated aluminum		
		θ_{stat}	θ_a	θ_r	θ_{stat}	θ_a	θ_r
Phosphatization, 25 $^{\circ}$ C during 3 min	25 mm min $^{-1}$	< 10	ND	ND	95 \pm 2.0	98	28
Phosphatization, 25 $^{\circ}$ C during 3 min	125 mm min $^{-1}$				96 \pm 1.5	97	32
Alkaline etching, 25 $^{\circ}$ C during 10 s	25 mm min $^{-1}$	21	ND	ND	103 \pm 0.5	105	41
Alkaline etching, 25 $^{\circ}$ C during 10 s	125 mm min $^{-1}$				109 \pm 0.5	108	45
Alkaline etching, 25 $^{\circ}$ C during 60 s	25 mm min $^{-1}$	20	ND	ND	98 \pm 1.5	102	35
Alkaline etching, 25 $^{\circ}$ C during 60 s	125 mm min $^{-1}$				100 \pm 0.6	104	32
Only degreasing	25 mm min $^{-1}$	69	64	40	98 \pm 2.5	99	38
Only degreasing	125 mm min $^{-1}$				96 \pm 2.6	98	42

ND = not determined, due to very low static contact angle values

($R_a = 6.8$ nm), relatively to the coating deposited at 25 mm min $^{-1}$. However, the roughness effects cannot explain the variation in contact angles for different pre-treatment conditions, as the chemical surface modification seems to be predominant. The samples that were pre-treated with alkaline etching for shorter and/or longer times and subsequently coated at 25 or 125 mm min $^{-1}$, have lower hydrophobicity with contact angles of 98 to 100 $^{\circ}$. Based on these results, the aluminum pre-treatment and coating conditions have important influences on the hydrophobicity of the final polymer coating. The highest contact angles were obtained for samples after alkaline etching at 25 $^{\circ}$ C, 10 s and dip-coating at high speed.

Corrosion tests

The results of salt-spray corrosion tests for uncoated aluminum samples (reference samples) are illustrated in Figure S3, indicating severe corrosion signs on the alkaline etched and degreased aluminum surfaces after a maximum exposure time of 480 h. Other evaluations after shorter times are not explicitly shown: in summary, severe corrosion starts on alkaline etched samples (with etching time 1 minute) after 120 hours, and on alkaline etched samples (with etching time 10 seconds) after 240 hours, while the degreased samples remain non-corroded until 360 hours exposure time. It can be concluded that in the first hours of the test, the samples are more affected by corrosion as they have been etched for longer times. This can be understood in parallel with the previous study on influences of substrate preparation, where the aluminum surfaces are homogeneous after short etching times and they become affected by intermetallic deposits after longer times. It is known that the presence of intermetallic particles at the surface affect the corrosion resistance, due to localized corrosion.⁴⁴

For the aluminum samples with a polymer coating (30 wt.% SMI/SoyO nanoparticles, 50 wt.% SB-latex and 20 wt.% carnauba wax), the corrosion was visually evaluated after phosphatization (Figure S4) and alkaline etching (25 $^{\circ}$ C, 1 min) (Figure S5). During dip-coating, the upper parts of the samples were not coated as they were clamped in the coating device. The polymer coating was deposited on the lower parts of the samples (both sides) upon withdrawal of the specimen from the coating dispersion.

From visual inspection of the corroded surfaces, both aluminum pre-treatment conditions are unfavourable for the quality of the deposited coating and consequently do not provide good corrosion resistance: even after short exposure times of only 120 hours, the coated samples have severe corrosion marks. In general, the alkaline-etched samples that were coated at high speed provide some better resistance than the coating deposited at low speed. The high-speed coated samples have a lower coating thickness, but they have slightly higher roughness and water contact angles.

The best corrosion resistance was observed for coated samples after alkaline etching (25 $^{\circ}$ C, 10 s), as shown in Figure 7. The corrosion of the coated samples was visually evaluated after 120, 240, 360 and 480 hours exposure time, for samples coated at low and high speed. From these tests, we can observe good corrosion resistance over 240 hours (Figure 7a, 7b). After 360 to 480 hours, weak localized corrosion appears on the sample coated at slow speed (Figure 7c), as observed by detachment of the coating from the substrate. The delamination is typical for corrosion of organic coatings and paints.⁴⁵ The sample that was alkaline etched at 25 $^{\circ}$ C during 10 seconds and then coated at 125 mm min $^{-1}$, has not suffered any corrosion damage (Figure 7d): this substrate preparation and coating condition provides the best coating quality for corrosion resistance.

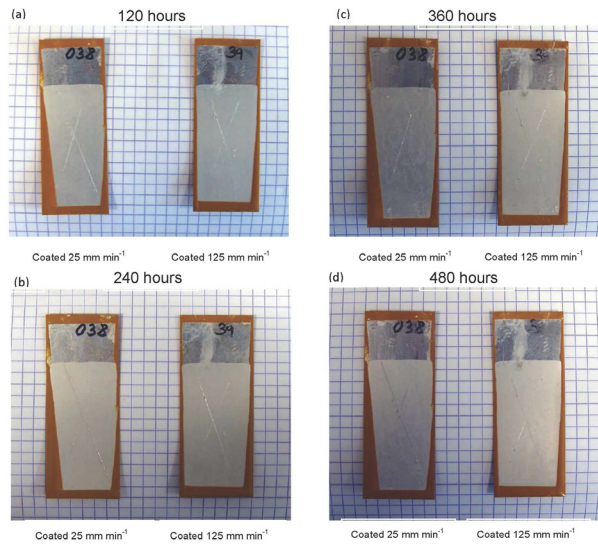


Figure 7. Corrosion test results for “best” alkaline etched samples (25 °C, 10 s) coated at slow speed and high speed after different exposure times, (a) 120 h, (b) 240 h, (c) 360 h, (d) 480 h.

Based on these results, it is concluded that alkaline etching (25 °C, 10 s) is the best pre-treatment and a high dip-coating speed significantly improves the corrosion resistance, in parallel with the values of contact angles and surface roughness. However, the long alkaline etching times do not provide sufficient corrosion resistance.

Contact angle measurements

After the 20-day corrosion test, the static water contact angles were measured on uncoated and coated aluminum samples with different values on corroded and non-corroded areas. The contact angles for samples that were pre-treated under different conditions and subsequently coated at 25 or 125 mm min⁻¹ are given in Table 6. Due to smaller available surface areas, the contact angle measurements

were averaged over 3 (or 2) measurements (instead on 10 before corrosion). The standard deviation on the contact angle values is rather high, mainly on the corroded areas due to the more irregular surface properties after exposure.

In absence of any coating, the samples remain hydrophilic after corrosion and the contact angles are so low (< 10°) that the drop spreads all over the surface. This means that the formation of corrosion products does not directly contribute to the formation of a hydrophobic barrier layer.

For corroded samples with phosphate pre-treatment and polymer coating, there is a significant difference in contact angles on corroded and non-corroded areas. The contact angles of 51 ± 11.5° to 36 ± 9.3° on corroded areas are higher than for corroded areas on the non-coated samples, but it does not provide hydrophobic protection. Otherwise, the contact angles of 87 ± 8.4° to 89 ± 8.5° on the non-corroded sample areas are relatively higher, as the coating remains intact and still provides some hydrophobic protection preventing further corrosion.

For corroded samples with alkaline pre-treatment and polymer coating, the contact angles on non-corroded areas are higher than on corroded areas. In particular, the contact angles on the non-corroded areas remain above 90° and provide hydrophobic protection. The contact angle in the non-corroded zones remains the highest (101°) after alkaline etching at 25 °C, 10 s and consequently provides best hydrophobic protection. Moreover, the standard deviation in contact angles over the non-corroded areas for the alkaline etched samples at 25 °C, 10 s is relatively low (± 2.1 to ± 4.4°), as an indication that those coatings are most homogeneous. The samples that were pre-treated with longer alkaline etching times have lower contact angles on the non-corroded areas (96°) and large standard deviation over the corroded areas (± 16 to ± 19°). Only two measurements could be taken on the non-corroded areas

Table 6. Static water contact angles (°) after a 20-day corrosion test on aluminum samples with different pre-treatments and coating conditions (values measured on corroded and non-corroded areas)

Aluminum pre-treatment	Coating condition	Static water contact angle θ_{stat} / degree	
		Corroded area	Non-corroded area
Phosphatization, 25°C during 3 min	Non-coated	< 10	< 10
Phosphatization, 25°C during 3 min	25 mm min ⁻¹	51 ± 11.5	87 ± 8.4
Phosphatization, 25°C during 3 min	125 mm min ⁻¹	36 ± 9.3	89 ± 8.5
Alkaline etching, 25°C during 10 s	25 mm min ⁻¹	46 ± 10.7	100 ± 4.4
Alkaline etching, 25°C during 10 s	125 mm min ⁻¹	76 ± 15.8	101 ± 2.1
Alkaline etching, 25°C during 60 s	25 mm min ⁻¹	70 ± 16.1	96 ± 6.5
Alkaline etching, 25°C during 60 s	125 mm min ⁻¹	79 ± 19.8	96 ± 5.7
Only degreasing	25 mm min ⁻¹	79 ± 19.8	95 ± 8.7
Only degreasing	125 mm min ⁻¹	84 ± 22.9	95 ± 9.7

because the sample was too much corroded and the surfaces were inhomogeneous. Depending on the coating parameters of alkaline-etched samples, the contact angles on corroded areas are the highest for coatings that were deposited at high dip-coating speed. While the standard deviation on contact angles for alkaline-etched coated samples is only $\pm 6.3^\circ$ in average, it is higher on phosphatized samples with a value of $\pm 9.3^\circ$. This means that the coating on alkaline-etched samples resists corrosion in a more uniform way than those on phosphatized samples. Therefore, the best conditions for hydrophobicity and corrosion protection of the polymer coating on aluminum are as follows: alkaline sample pre-treatment (25 °C, 10 s) and high dip-coating speed (125 mm min⁻¹).

For the corroded samples that were pre-treated by degreasing, the contact angles for corroded areas are generally higher than the ones for corroded areas in etched and phosphatized samples. This is not due to a better quality of the coating on the degreased samples, but can be explained by the formation of a specific surface morphology after corrosion: some corroded areas show a characteristic rough profile due to the deposition of corrosion products which serves as an anchor to the drop, keeping it well located on the sample and maintaining a relatively high contact angle.

Coating thickness measurements

The changes in thickness of the polymer coating on different aluminum substrates were calculated from thickness measurements before and after a 20-day corrosion test. The measurements of coating thickness take into account the statistical variation over the sample by performing ten thickness measurements per sample, including five measurements at the front and five measurements at the back side of the samples (Minitest

2000). The absolute changes in coating thickness are calculated as the difference of the average thickness per sample side before and after corrosion, as given in Table 7.

For all samples, the polymer coating thickness has increased after corrosion (+ value), which can likely be explained by two phenomena: (i) the first and most important one, is the fact that water molecules diffuse into the polymer coating and cause swelling of the polymer layer, and (ii) a second reason, is the appearance of corrosion products over the coating layer and the formation of a thicker salt layer. The different changes in coating thickness on the front and back side of the samples may be attributed to the positioning of the surface in the salt spraying test (see Figure S2). There might be a significant difference in thickness change on both sides, but the general trends comparing both sample sides are comparable.

The polymer coatings that were applied under ideal conditions, according to previous analysis (alkaline etching, 25 °C, 10 s; coating 125 mm min⁻¹), show the smallest dimensional change (+2.1 μm) with good homogeneity on front and back side. Consequently, the visual observations of optimum corrosion resistance are confirmed by the quantitative data of coating thickness change. Based on these findings, the protective layer on samples coated at high speed is relatively thin with a thickness of 6.5 μm (Table 4), but it may provide good corrosion resistance in parallel with the highest values for contact angle of 109° (Table 5). For aluminum substrates with the same pre-treatment (alkaline etching, 25 °C, 10 s), the hydrophobicity of coatings deposited at high speeds may be enhanced by the slightly higher average roughness at the nanoscale ($R_a = 6.8$ nm, Table 4) compared to the samples coated at lower speeds ($R_a = 4.3$ nm, Table 4). However, a direct correlation between contact angle and corrosion resistance remains difficult to draw and hydrophobicity might only provide a first indication for corrosion resistance. While the

Table 7. Change in polymer coating thickness after a 20-day corrosion test on aluminum samples with different pre-treatments and coating conditions

Aluminum pre-treatment	Coating condition	Coating thickness change at front side / μm	Coating thickness change at back side / μm
Phosphatization, 25 °C during 3 min	Non-coated	–	–
Phosphatization, 25 °C during 3 min	25 mm min ⁻¹	+2.4	+6.2
Phosphatization, 25 °C during 3 min	125 mm min ⁻¹	+14.1	+20.9
Alkaline etching, 25 °C during 10 s	25 mm min ⁻¹	+19.0	+12.6
Alkaline etching, 25 °C during 10 s	125 mm min ⁻¹	+2.1	+2.2
Alkaline etching, 25 °C during 60 s	25 mm min ⁻¹	+5.5	+3.3
Alkaline etching, 25 °C during 60 s	125 mm min ⁻¹	+28.8	+11.8
Only degreasing	25 mm min ⁻¹	+45.8	+19.3
Only degreasing	125 mm min ⁻¹	+3.4	+11.2

determined hydrophobicity acts in the presence of water and air (3-phase system), corrosion may proceed not only in a humid atmosphere, but also under immersion of the sample in a corrosive solution.

The data in this study demonstrate the corrosive protection of aluminum surfaces through the application of a polymer coating layer including nanoparticles containing plant oil, together with a latex and carnauba wax. Moreover, the aluminum substrate preparation and the coating deposition conditions have a strong influence on the hydrophobicity, coating thickness and resulting corrosion resistance. The corrosion behaviour of reference coatings with nanoparticle layers not including plant oils were not tested, as these coatings do not form continuous protective layers after drying. This was previously observed while applying the pure nanoparticle coatings on paper substrates.³⁹

Conclusions

A polymer coating with organic nanoparticles, carnauba wax and styrene/butadiene latex was evaluated to improve the corrosion resistance of aluminum substrates, in parallel with the optimization of the hydrophobic surface properties. Different aqueous dispersions of styrene maleimide nanoparticles with chemically bonded vegetable oils (SMI/oil) were synthesized by imidization of poly(styrene-*co*-maleic anhydride) in presence of different vegetable oils. Various compositions were screened as coating substances in order to provide high degree of imidization, resulting in homogeneous coatings with relatively high contact angles, low contents of free oil and good stability over time. In conclusion, the incorporation of soy oil is most appropriate in parallel with the high reactivity of poly-unsaturated oils and chemical binding of the oil to the organic phase, as confirmed by Raman spectroscopy.

After varying the coating composition, the hydrophobicity and long-term stability of the coating was optimized, resulting in a polymer coating with following components: 30 wt.% SMI/oil, 20 wt.% carnauba wax, and 50 wt.% latex. As a result, the latter polymer coating has a homogeneous and 'closed' structure with a somewhat lower average surface roughness than the pure SMI/oil nanoparticle coating, and it shows a maximum contact angle of 109°. Other coating compositions did not result in a homogeneous structure, or did not show long-term stability due to migration of the coating components. In parallel, different pre-treatment conditions of the aluminum surfaces were investigated and optimized for alkaline etching at 25 °C for 10 s. The etching temperatures did

not significantly affect to the morphology of the surface, while the amount of intermetallic particles on the surface was minimized for intermediate etching times.

The polymer coating with best corrosion resistance was applied on alkaline-etched aluminum substrates (25 °C, 10 s) at a high dip-coating speed of 125 mm min⁻¹. The good corrosion resistance was quantitatively confirmed by small changes in coating thickness and hydrophobicity after corrosion. In parallel, this coating is relatively thin compared with a coating that was applied at low speed, but its hydrophobicity may be enhanced by the slightly higher average roughness at the nanoscale when comparing aluminum substrates that were etched under the same conditions. As such, a polymer coating with efficient hydrophobic protection may contribute to better corrosion protection.

Acknowledgments

P. Samyn acknowledges the Robert Bosch Foundation for financial support. Dr D. Stanssens at Topchim N.V. is acknowledged for production of SMI/oil nanoparticles. Mr P. Mast provided technical assistance for corrosion tests.

References

1. Sharmin, E.; Ahmad, S.; Zafar, F. In *Corrosion Resistance*; Shih, H., ed.; InTech: Rijeka, Croatia, 2012, ch. 20.
2. El-Lateef, H. M.; Aliyeva, L. I.; Abbasov, V. M.; Ismayilov, T. A.; Ismayilova, X. R.; *Chemistry J.* **2012**, *2*, 37.
3. Deflorian, F.; Fedel, M.; Di Gianni, A.; Bongiovanni, R.; Turri, S.; *Corros. Eng. Sci. Technol.* **2008**, *43*, 81.
4. Sathyanarayana, A.; Bambole, V.; Sabharwal, S.; Mahanwar, P.; *Pigm. Res. Technol.* **2013**, *42*, 362.
5. Rathish, R. J.; Dorothy, R.; Joany, R. M.; Pandiarajan, M.; Rajendran, S.; *Eur. Chem. Bull.* **2013**, *2*, 965.
6. Choi, H.; Song, Y. K.; Kim, K. Y.; Park, J. M.; *Surf. Coat. Technol.* **2012**, *206*, 2354.
7. Raps, D.; Hack, T.; Kolb, M.; Zheludkevich, M. L.; Nuyken, O. In *ACS Symposium Series Vol. 1050: Smart Coatings III*; Baghdachi, J.; Provder, T., eds.; ACS: Washington, DC, USA, 2010, 165.
8. Borisova, D.; Möhwald, H.; Shchukin, D. G.; *ACS Nano* **2011**, *5*, 1939.
9. Norzita, N.; Haziq, M.; Zurina, M.; *Int. J. Chem. Environ. Eng.* **2012**, *3*, 267.
10. Feil, F.; Fürbeth, W.; Schütze, M.; *Surf. Eng.* **2008**, *24*, 198.
11. Al-Thabaiti, S. A.; Malik, M. A.; Al-Youbi, A. A. O.; Khan, Z.; Hussain, J. I.; *Int. J. Electrochem. Sci.* **2013**, *8*, 204.
12. Atta, A. M.; El-Mahdy, G. A.; Al-Lohedan, H. A.; *Int. J. Electrochem. Sci.* **2013**, *8*, 4873.

13. Shanaghi, A.; Sabour, A. R.; Shahrabi, T.; Aliofkhaeze, M.; *Prot. Met. Phys. Chem. Surf.* **2009**, *45*, 305.
14. Zhang, X.; Wang, F.; Du, Y.; *Surf. Coat. Technol.* **2007**, *201*, 7241.
15. Gao, G.; Wu, H.; He, R.; Cui, D.; *Corros. Sci.* **2010**, *52*, 2804.
16. Ramezanzadeh, B.; Attar, M. M.; *Mater. Chem. Phys.* **2011**, *130*, 1208.
17. Behzadnasab, M.; Mirabedini, S. M.; Kabiri, K.; Jamali, S.; *Corros. Sci.* **2011**, *53*, 89.
18. Chandrappa, K. G.; Venkatesha, T. V.; *Mater. Corros.* **2013**, *64*, 831.
19. Li, Y.; Fedkiw, P. S.; *Electrochim. Acta* **2007**, *52*, 2471.
20. Sharmila, R.; Selvakumar, N.; Jeyasubramanian, K.; *Mater. Lett.* **2013**, *91*, 78.
21. Zhang, Z.; Chen, S.; Ren, H.; Zhou, J.; *Appl. Surf. Sci.* **2009**, *255*, 4950.
22. Lewis, O.; Critchlow, G.; Wilcox, G.; Dezeeuw, A.; Sander, J.; *Prog. Org. Coat.* **2012**, *73*, 88.
23. Liu, J. H.; Zhan, Z. W.; Li, S. M.; Yu, M.; *J. Central South University* **2012**, *19*, 45.
24. Zhang, X. L.; Zhang, S. L.; Lei, Y.; *Metal Finishing*, **2012**, *110*, 24.
25. Shi, X.; Nguyen, T. A.; Suo, Z.; Liu, Y.; Avci, R.; *Surf. Coat. Technol.* **2009**, *204*, 237.
26. Madhankumar, A.; Nagarajan, S.; Rajendran, N.; Nishimura, T.; *Met. Mater. Int.* **2012**, *18*, 965.
27. Mahulikar, P. P.; Jadhav, R. S.; Hundiwale, D. G.; *Iran. Polym. J.* **2011**, *20*, 367.
28. Li, D.; Chen, S.; Zhao, S.; Ma, H.; *Colloids Surf. A* **2006**, *273*, 16.
29. Zaharescu, M.; Predoana, L.; Barau, A.; *Corros. Sci.* **2009**, *51*, 1998.
30. Lei, J. P.; Huang, H.; Dong, X. L.; Zhu, X. G.; Lu, B.; Lei, M. K.; *J. Nanosci. Nanotechnol.* **2009**, *12*, 7503.
31. Toloei, A.; Atashin, S.; Bahrololoom, M. E.; *Mater. Sci.* **2013**, *2013*, ID 648246.
32. Keyoonwong, W.; Guo, Y.; Kubouchi, M.; Aoki, S.; Sakai, T.; *Int. J. Corros.* **2012**, *2012*, ID 924283.
33. Truc, T. A.; Hang, T. T. X.; Oanh, V. K.; Dantras, E.; Lacabanne, C.; Oquab, D.; Pébère, N.; *Surf. Coat. Technol.* **2008**, *202*, 4945.
34. Olivier, M. G.; Fedel, M.; Sciamanna, V.; Vandermiers, C.; Motte, C.; Poelman, M.; Deflorian, F.; *Prog. Org. Coat.* **2011**, *72*, 15.
35. Li, X. G.; Huang, M. R.; Zeng, J. F.; Zhu, M. F.; *Colloids Surf. A* **2004**, *248*, 111.
36. Chen, F.; Liu, P.; *ACS Appl. Mater. Interfaces* **2011**, *3*, 2694.
37. Zubillaga, O.; Cano, F. J.; Azkarate, I.; Molchan, I. S.; Thompson, G. E.; Cabral, A. M.; Morais, P. J.; *Surf. Coat. Technol.* **2008**, *202*, 5936.
38. Höhne, S.; Blank, C.; Mensch, A.; Thieme, M.; Frenzel, R.; Worch, H.; Müller, M.; Simon, F.; *Macromol. Chem. Phys.* **2009**, *210*, 1263.
39. Samyn, P.; Deconinck, M.; Schoukens, G.; Stanssens, D.; Vonck, L.; Van den Abbeele, H.; *Prog. Org. Coat.* **2011**, *69*, 442.
40. Samyn, P.; Schoukens, G.; Stanssens, D.; Vonck, L.; Van den Abbeele, H.; *J. Nanopart. Res.* **2012**, *8*, 1075.
41. Overbeek, A.; *J. Coat. Technol. Res.* **2010**, *7*, 1.
42. Bajat, J. B.; Popic, J. P.; Miskovic-Stankovica, V. B.; *Prog. Org. Coat.* **2010**, *69*, 316.
43. Lunder, O.; Heen, K. F.; Nisancioglu, K.; *Corrosion* **2004**, *60*, 622.
44. Buchheit, R. G.; Boger, R. K.; Carroll, M. C.; Leard, R. M.; Paglia, C.; Searles, J. L.; *JOM* **2001**, *53*, 29.
45. Schweitzer, P. A.; *Paint and Coatings: Applications and corrosion resistance*; CRC Press, Taylor and Francis Group: Boca Raton, USA, 2006.

Submitted: November 17, 2013

Published online: April 4, 2014